A new alcohol-soluble dye-tetraphenyl porphyrin functionalized copolymer: Inside the role as a third component/cathode interlayer in halogen-free OSCs

Martina Marinelli [a,*], Massimiliano Lanzi [a,*], Debora Quadretti [a], Yasamin Ziai [b], Filippo Pierini [b], Alberto Zanelli [c], Riccardo Medri [a], Elisabetta Salatelli [a,*]

[a] Dpt. of Industrial Chemistry "Toso Montanari", University of Bologna, Viale Risorgimento 4, 40136 Bologna, Italy
[b] Dpt. of Biosystem and Soft Matter, Institute of Fundamental Technological Research, IPPT-PAN, Polish Academy of Science, ul. Pawińskiego 5B, 02-106 Warsaw, Poland
[c] Institute for Organic Synthesis and Photoreactivity (ISOF), National Research Council (CNR), Via P. Gobetti 101, 40129 Bologna, Italy

ARTICLE INFO

ABSTRACT

Development and step-by-step characterizations of a novel cationic thiophene based copolymer (**P1buP**), including ionic phosphonium salt and dye-tetraphenylporphyrin (TPP) moiety in side chains, with an iconic property of solubility in a wide range of polar solvents is reported. Synthesized by using simple, low-cost, and straightforward procedures, the material is used to fabricate completely halogen-free (i.e., from ethanol) ternary organic solar cells (OSCs), in the presence of an alcohol-soluble ionic 3,4-dialkoxythiophene based homopolymer (**P2buP**) and a serinol-fullerene derivative (C_{60}-**Ser**). Indeed, thanks to co-sensitization techniques, where multiple dyes harvest different parts of the solar spectrum, the power conversion efficiency of the best final device dramatically increases up to nearly 5.0%, as the light absorption is usually optimized. Additionally, since the use of a cathode interlayer in OSCs also plays a pivotal role in electron extraction and device stability, a possible application of the ionic TPP material as the interfacial layer is also investigated. Furthermore, to improve and optimize the best performing device, a successful post-metalation with Zn of the porphyrin core is carried out, and a ternary OSC (P1buP:P2buP:C_{60}-Ser = 0.33:0.67:1 *w*/w) is fabricated, resulting in a photo-conversion efficiency (PCE) of ~6.0%.

1. Introduction

Solar energy and the development of new photovoltaic technologies (PVs) are valid eco-friendly solutions to prevent today's energy shortage and environmental pollution results. In particular, organic solar cells (OSCs) are among the best promising devices for clean energy production, firstly because they do not use critical raw materials [1], such as high purity silicon or gallium, then due to their lightweight, flexibility, low-cost manufacturing, as well as high tune-ability, large-area coverage, semitransparent fabrication, and safe waste disposal [2–4]. A typical OSC is commonly made by a bi-continuous and interpenetrating electron donor (ED, i.e., π-conjugated polymer) and electron acceptor (EA, i.e., fullerene derivative) composite blend, which acts as a photo-active layer and is placed between an anode (i.e., Indium Tin Oxide [ITO]) and a cathode (i.e., Al) [5]. Up to now, the photoconversion efficiency (PCE) of OSCs has exceeded 18% [6–8]. Indeed, since efficiency is still the primary factor, much effort has been made to boost the photovoltaic performances of those bulk-heterojunction (BHJ) OSCs, acting both on the design of new high-performance active materials, morphology optimization, and device engineering [9–12].

The synthesis and use of a dye sensitizer (i.e., porphyrin and/or metal-porphyrin derivatives) is a well-known and valid strategy, since
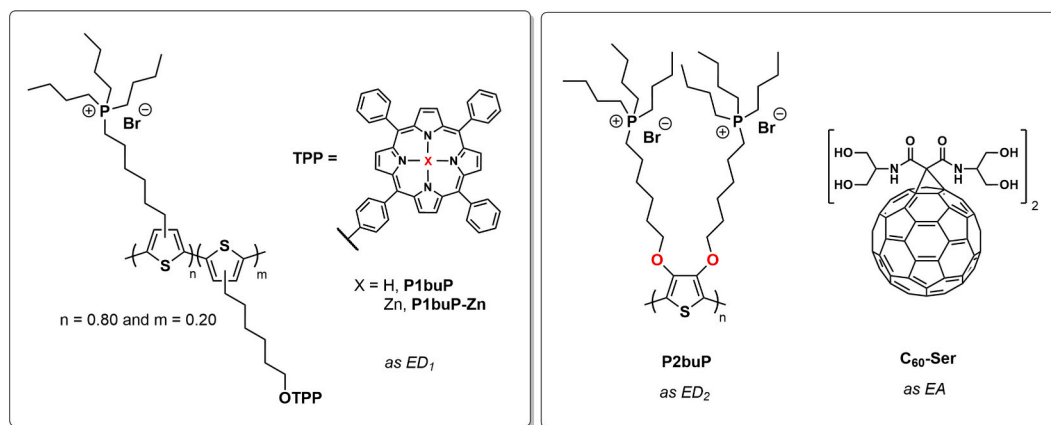
Fig. 1. Overview of the alcohol-soluble ED (**P1buP** and **P2buP**) and EA (**C$_{60}$-Ser**) BHJ blend components.

they are large planar π-aromatic systems, thermally and photochemically stable photoactive components, and typically have broad absorption regions owing to their Soret and Q bands. Moreover, such derivatives can be both blended with ED/EA materials or directly anchored to the π-conjugated polymeric backbone [13–15]. In order to enhance their light-harvesting properties in the visible and NIR regions, these derivatives could be paired with a solution-processable 3,4-dialkoxythiophene based polymers as second ED photoactive components. In fact, not only does the stronger electron donor ability of double oxygen reduce the energy band gap of the material, but S—O noncovalent interaction could also provide a better planarity and modulate the final morphology of the blend [16,17]. Therefore, the new concept of co-sensitization and development of ternary OSCs, obtained by using three photoactive materials with complementary absorption profiles, is of great interest [18,19]. The introduction of a third component typically broadens the light harvesting capability and enhances the charge transfer and/or transport properties, thus improving the final device performance. Besides, the third element seems to act as a morphology regulator, since a better stability (i.e., thermal and photochemical) and an optimized phase separation of the ternary blend can be obtained [15,19–21]. However, co-sensitization sometimes could also lead to difficulty in morphology control, thus producing an unexpected and complex morphology and, therefore an overall decrease in efficiency.

For this reason, the device architecture – especially interfacial engineering – is another aspect to focus on [22–24]. Anode/cathode interfacial materials (AIM/CIMs) or holes/electron transport layers (HTL/ETLs) are usually conjugated polyelectrolytes with polar and/or ionic side chains, which are placed between the active layer and the metal electrode. In addition to solving the rising quest for green solvents to be soluble and processable from alcohols and/or water, this class of materials can reduce the work function of the electrode metal and produce a favorable energy level alignment for an effective and better charge extraction. Besides, oxidation phenomena are prevented and as a result, the long-term stability of the device is improved [25–27].

Therefore, we herein report the synthesis of two novel cationic and alcohol/water-soluble conjugated thiophene-based materials. In particular, the dye-tetraphenylporphyrin (TPP) functionalized copolymer poly {3-(6-tributylphosphoniumhexyl)thiophene-co-3-[5-(4-phenoxy)-10,15,20-triphenylporphyrinyl]hexylthiophene bromide} (**P1buP**) and the 3,4-dialkoxythiophene based homopolymer poly[3,4-(6,6′-tributylphosphoniumhexyloxy)thiophene] bromide] (**P2buP**) – both with ionic phosphonium salts in the side chains – have been prepared by a post-functionalization approach on the precursor polymers poly{3-(6-bromohexyl)thiophene-co-3-[5-(4-phenoxy)-10,15,20-triphenylporphyrinyl]hexylthiophene} (**P1**) and poly[3,4-(6,6′-bromohexyloxy) thiophene] (**P2**). All the synthesized materials were fully characterized

by nuclear magnetic resonance (^{1}H NMR, ^{13}C NMR and ^{31}P NMR), infrared (FT-IR) and ultraviolet-visible/photoluminescence (UV–Vis and PL) spectroscopy, as well as thermal analysis (TGA and DSC), cyclic voltammetry (CV), atomic force microscopy (AFM), and external quantum efficiency (EQE). The ionic polymers were then tested as photoactive ED materials in halogen-free (i.e., ethanol) ternary BHJ OSCs, in the presence of an alcohol-soluble serinol-fullerene (**C$_{60}$-Ser**) derivative as an EA counterpart (Fig. 1). Moreover, to investigate a possible role in the process of device engineering, the alcohol-soluble TPP functionalized copolymer was also tested as cathode interfacial layer in a bicomponent BHJ OSC made of **P2buP:C$_{60}$-Ser** as active layer. Finally, to improve and optimize the best performing device, the ionic TPP substituted copolymer was subsequently metalated with Zn and tested in a ternary BHJ OSCs (**P1buP-Zn:P2buP:C$_{60}$-Ser** = 0.33:0.67:1 *w/*w), achieving even higher PCE value (~ 6.0%) but still maintaining an environmentally friendly approach.

2. Experimental section

2.1. Materials and methods

All commercial chemicals and solvents were used as supplied, unless otherwise noted. 1,6-Hexanediol (99%), hydrochloric acid (HCl, ≥37%), *p*-toluenesulfonic monohydrate acid (pTsOH•H$_2$O, ≥99%), sodium bicarbonate (NaHCO$_3$, puriss.), sodium sulphate (Na$_2$SO$_4$, anhydrous), tributyl phosphine (Pbu$_3$, 97%), zinc acetate dihydrate (Zn(OAc)$_2$ • H$_2$O, ≥98%), poly(9,9-bis(3′-(*N,N*-dimethyl)-N-ethylammoinium-propyl-2,7-fluorene)-alt-2,7-(9,9-dioctylfluorene))dibromide (PFN-Br), toluene (C$_7$H$_8$, >99.9%), ethyl acetate (EtOAc, >99.5%), petroleum ether (PE, >90%), hexane (C$_6$H$_{13}$, >99.0%), tetrahydrofuran (THF, >99.9%) and diethyl ether (Et$_2$O, >99.5%) were purchased from Sigma Aldrich Chemical Co. (USA). Hydrobromic acid (HBr, 48%), ferric trichloride (FeCl$_3$, ≥98%), phosphorus pentoxide (P$_2$O$_5$, 99%) and nitromethane (CH$_3$NO$_2$, ≥98.5%) from Fluka (Switzerland). Dichloromethane (CH$_2$Cl$_2$, 99%), chloroform (CHCl$_3$, 99.0–99.4%) and methanol (MeOH, >99.8%) from Honeywell (Germany). Diethyl ether (Et$_2$O) and tetrahydrofuran (THF) were freshly distilled before use to remove the stabilizer, while anhydrous chloroform (CHCl$_3$) was distilled over P$_2$O$_5$ and stored over molecular sieves. The synthesis and characterization of 3-(6-bromohexyl)thiophene (**1a**) [28] and 3-[6-(4-phenoxy)-10,15,20-triphenylporphyrinyl]hexylthiophene (**1b**) [29] as starting monomers, in addition to malonodiserinolamide fullerene (**C$_{60}$-Ser**) [30] as electron-acceptor counterpart were previously reported. Monomer 3,4-(6,6′-bromohexyloxy)thiophene (**2**) was synthesized according to literature methods [16,31], starting from commercially available 3,4-dimethoxythiophene (Sigma Aldrich, 98%) and 6-bromo-1-hexanol ((**B6OH**), prepared according to ref. [32]). Precursor (**P1**
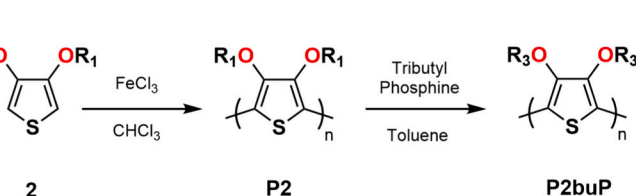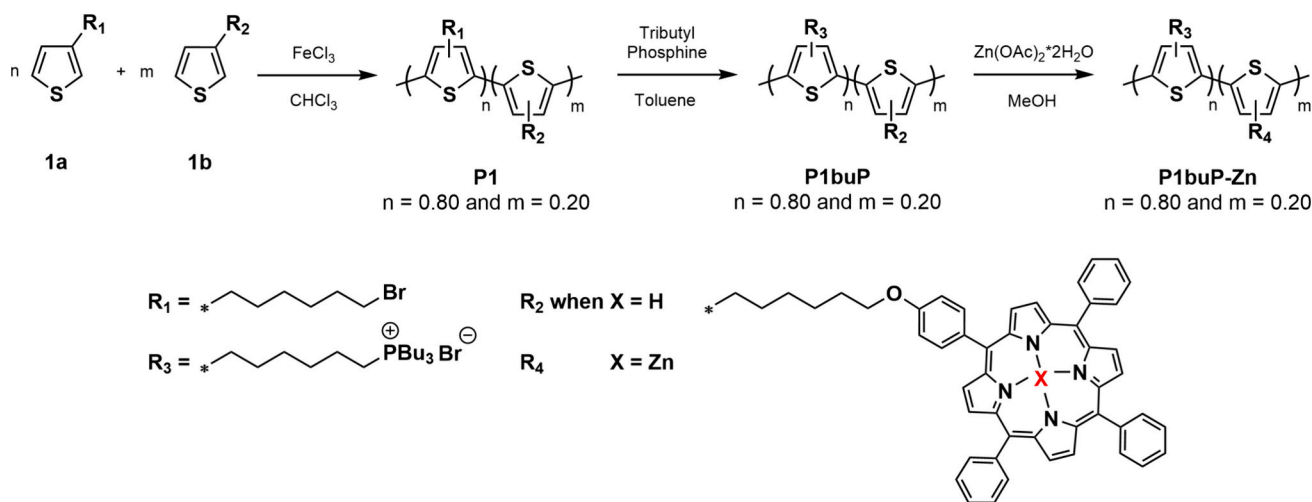
Scheme 1. Synthetic route to obtain the precursor and ionic thiophene-based materials.

and **P2**) [29,33] and ionic (**P1buP** and **P2buP**) [30,34] polymers/co-polymers were synthesized according to literature methods. Metalation with Zn to obtain **P1buP-Zn** was performed according to modified literature method [35,36]. All synthetic details are given in the Supporting Information. All air- or moisture-sensitive reactions were performed under an inert (N_2) atmosphere in flame-dried glassware.

2.2. Instruments

The NMR (^{1}H, ^{13}C and ^{31}P) spectra were recorded on a Varian Mercury Plus 400 (400 MHz) spectrometer, operating at room temperature. Chemical shifts are given in ppm and referenced in the deuterated solvents (CDCl$_3$: δ = 7.26 ppm for ^{1}H and 77.00 ppm for ^{13}C; CD$_3$OD: δ = 3.31 ppm for ^{1}H and 49.10 ppm for ^{13}C). The following abbreviations have been used for multiplicity assignments: "s" for singlet, "d" for doublet, "t" for triplet, "m" for multiplet, and "br" for broad. High-resolution mass spectroscopy (ESI-HRMS) spectra were recorded on a Waters Xevo Q-TOF.

Molecular weights of precursor polymers (**P1** and **P2**) were measured by gel permeation chromatography (GPC) on a HPLC Lab Flow 2000 apparatus equipped with a Rheodyne 7725i injector, a Phenomenex Phenogel MXM 5 μm mixed bed column, and an RI K-2301 KNAUER detector, using monodisperse polystyrene as standards and THF as the eluent. Solutions of ca. 1 mg/mL were prepared and filtered over a 0.45-μm pore size filter, just before measurements.

Thermogravimetric analyses (TGA) were conducted on NETZSCH TG 209 F1 Libra (**P1buP**) and a TA Instruments Q600 apparatus (**P2buP**) operating in air flux, to determine the sample decomposition temperatures (from 30 °C to 600 °C, heating rate scan of 10 °C min^{-1}). A TA Instruments Q2000 differential scanning calorimeter (DSC) was used under a nitrogen atmosphere for the thermal analysis (from −20 to 200 °C, heating rate scan of 10 °C min^{-1}).

Absorption (UV–Vis) spectra of the different materials were acquired at room temperature on a Perkin Elmer Lambda 19 spectrophotometer, with a 1 cm path length quartz cell and ~ 10^{-5} M polymer solutions (CHCl$_3$ for **P1–2** and alcohols/water for **P1–2buP**). Thin film measurements were made on polymer samples or BHJ blends cast on quartz

slides by spray-coating deposition. Emission spectra of solutions and thin films on glass-substrate were recorded on an Edinburgh FLSP920 spectrometer equipped with a 450 W xenon arc lamp, double excitation and single emission monochromators, and a Peltier-cooled Hamamatsu R928P photomultiplier tube (185–850 nm). The wavelengths for the emission spectra were determined using the abs maxima. FT-IR spectra were recorded on KBr or Ge disks using a Perkin Elmer Spectrum One spectrophotometer.

Cyclic voltammetries (CVs) were performed at room temperature with an AMEL 5000 Electrochemical system, in an Ar purged mixture of 25% acetonitrile (CH$_3$CN, Carlo Erba RPE, distilled and stored on 3 A molecular sieves under Ar pressure) and 75% toluene (C$_7$H$_8$, Carlo Erba RPE, distilled in Rotavapor) solution of 0.1 mol L^{-1} tetrabutylammonium perchlorate ((C$_4$H$_9$)$_4$NClO$_4$, Fluka, electrochemical grade) as supporting electrolyte. Measurements were conducted using a three-compartment glass cell equipped with a Pt wire spiral and an aqueous saturated calomel electrode (SCE) as the auxiliary and reference electrodes, respectively. Polymer films were formed by drop-casting ionic polymer solutions in methanol on a 1 mm diameter Pt electrode. Potentials are referenced to the ferrocene/ferrocenium (FC$^+$/FC) couple, whose standard potential for the mixture is E°$_{[FC+/FC]}$ = 0.599 V vs. SCE, while the absolute potential is assumed 4.84 eV [37–39].

Atomic force microscopy (AFM, model Ntegra from NT-MDT) was employed to gather surface topography and phase image data of the blends. This equipment was supplied with a silicon cantilever (model NSG01 from NT-MDT, having a tip radius of 10 nm), and the measurements were conducted in a semi-contact mode, operating at a resonance frequency of 200 kHz, and each image was composed of 500 × 500 data points.

The current-voltage (J-V) characteristics of the prepared solar devices were measured in air at room temperature, with a digital source meter (Keithley 2401) under the illumination of an Abet Technologies LS150 Xenon Arc Lamp Source AM 1.5 Solar Simulator (100 mW/cm^2) calibrated with an ILT 1400-BL photometer. The external quantum efficiency (EQE) characterization was made by using a 7-SC Spec III Modularized Solar Cell Spectral Test System (SevenStar Optics, Beijing, PRC).

Table 1

Comparison of the physical and thermal characteristics of precursor and ionic polymeric derivatives.

	Reaction Yield (%)	Dyads Content (%)	Group Content (% mol)[a]	M_n (KDa)	X_n[b]	Đ[d]
P1	45	70 HT[a]	80 Br, 20 TPP	33.6[b]	95	1.7
P2	60	100 HH	100 Br	42.4[b]	96	1.5
P1buP	91	70 HT[a]	80 buP, 20 TPP	49.0[c]	95	1.7
P2buP	95	100 HH	100 buP	81.4[c]	96	1.5

[a] Determined by ^{1}H NMR; [b] Determined by GPC relative to polystyrene standards; [c] Calculated from the average polymerization degree of the corresponding precursor polymers; [d] Polydispersity index, determined by GPC; TPP = tetraphenylporphyrine, buP = tributylphosphine.

2.3. Device fabrication

The Indium Tin oxide (ITO) substrate (2 × 2 cm, surface resistance 21 Ω/sq) was etched at 60 °C for 15 min by using a 10% wt aqueous solution of HCl, to obtain an active area of 1.5 × 1.0 cm. The substrate was rinsed with distilled water, 2-propanol and dried with a nitrogen flow before use. The solution of poly(3,4-ethylenedioxythiophene): polystyrene sulfonic acid (PEDOT:PSS, 2.8 wt% dispersion in water, viscosity 20 cps) in 2-propanol (diluted 1:1 *v/v*) was sonicated for 30 min using an ultrasonic bath (Elmasonic S 30H), filtered on a Gooch G2 and then deposited by doctor blading technique (Sheen Instrument Model S265674) onto the previously treated ITO substrate, only leaving a small (0.5 × 1 cm) area uncovered at the opposite side of the previously etched area. The PEDOT:PSS film was annealed at 120 °C for 2 h under vacuum (Buchi GKR-50 glass oven, 10^{-3} mmHg). The active layer was deposited under ambient air conditions by spray-coating (Gohelper Mini Kit Airbrush, nozzle diameter 0.3 mm) of a solution made by mixing different weight ratios of **P1buP** or **P2buP** (as ED polymer) and **C$_{60}$-Ser** (as EA material) in 2.0 mL of EtOH/MeOH = 2/1, and then annealed in the glass oven under vacuum (10^{-3} mmHg) at 120 °C for 30 min. In case of bicomponent photoactive blend (**P2buP:C$_{60}$-Ser** = 1:1 *w/ w*), 1.0 mL of a solution of **P1buP** in EtOH (2 mg/mL) as cathode interlayer was also deposited by spray-coating and subsequently annealed at 120 °C for 30 min. Finally, 50 nm of Al was thermally evaporated by using an Edwards 6306 A coating system operating at 10^{-6} mmHg. The structure of the final devices, having a final active area of 1.0 × 1.0 cm^2, was composed of (i) ITO (80 nm)/PEDOT:PSS (100 nm)/photo active layer (150 nm)/Al (50 nm) or (ii) ITO (80 nm)/ PEDOT:PSS (100 nm)/photoactive layer (150 nm)/ionic polymer (20 nm)/Al (50 nm).

3. Results and discussion

3.1. Synthesis and physical characterization

Monomers 3-(6-bromohexyl)thiophene (**1a**) [28] and 3-[6-(4-phenoxy)-10,15,20-triphenylporphyrinyl]hexylthiophene (**1b**) [29] (Scheme 1) were synthesized according to literature methods. The new monomer 3,4-(6,6′-bromohexyloxy)thiophene (**2**) was synthesized by trans-etherification [16,31] of the commercially available 3,4-dimethoxythiophene, in the presence of 6-bromo-1-hexanol (B6OH) [32] and a catalytic amount of p-toluenesulfonic acid (for detailed procedures see Supporting Information). Both precursor materials were then obtained by oxidative coupling with iron chloride (FeCl$_3$) of the corresponding monomers, to give the dye-sensitized thiophene-based copolymer (**P1**) [29] and the homo-poly(dialkoxythiophene) (**P2**) [33].

P1 was obtained by direct *co*-polymerization of monomers **1a** and **1b** in the molar feed ratio of 4.1:1, respectively, and a head-to-tail (HT) dyads content of 70%. Indeed, to prevent self-aggregation phenomena typically observed in this class of materials, a partially functionalized and not completely regioregular derivative – with the TPP moiety

anchored to but electronically insulated from the polyconjugated thiophene backbone – was synthesized. Whereas for **P2**, a completely regioregular precursor material was obtained, thanks to the symmetrical structure of the 3,4-disubstituted monomer. Besides, in addition to being well-soluble in most common organic solvents (i.e., THF or CHCl$_3$), both precursor materials display high molecular weights (M$_n$) and uniformity in chain length, as average polymerization degrees (X$_n$, Table 1) of **P1** and **P2** are of comparable magnitude. Cationic, and therefore water/ alcohol soluble materials (**P1buP** and **P2buP**) were then synthesized according to previous literature methods [30,40], by post-functionalization with tributyl phosphine of the bromoalkylic side chains of the precursor derivatives. Substitution reaction with phosphines generally leads to a complete post-functionalization, thus increasing the solubility in water and polar solvents, without affecting the final regioregularity degree of the material. Indeed, both **P1buP** and **P2buP** derived to be fully soluble in water and a wide range of alcohols (i.e., methanol, ethanol, *n*-propanol, and *i*-propanol). An overview and comparison of the precursor and ionic derivatives' characteristics is reported in Table 1.

Finally, as metalation typically affects the optical and electrochemical properties of porphyrin derivatives, a portion of **P1buP** was subsequently complexed with Zn^{2+} to obtain **P1buP-Zn** (Scheme 1). Due to the ionic nature of the synthesized TPP derivative, the reaction was successfully performed at room temperature in MeOH and using stoichiometric zinc acetate dihydrate, according to the conditions reported in the experimental section (for detailed procedures refer to Supporting Information, Section I). The successful metalation, probably thanks to the strong reduction of the π-π stacking interaction of the porphyrin moieties, further improves the solubility of **P1buP-Zn** in highly polar solvents such as alcohols or water.

3.2. NMR characterization

All precursors and monomers were characterized by ^{1}H NMR, ^{13}C NMR and mass spectroscopy to determine their chemical structure and purity degree (Fig. S1-S2). The occurrence of the polymerization and post-functionalization reactions with tributyl phosphine was proved by ^{1}H NMR (Fig. S3-S4), as well as ^{31}P NMR (Fig. S5-S6).

The copolymerization of **P1** is proved by splitting the signal resonance related to the methylenic protons in α to the thiophenic ring (Fig. S3A). While the successful homopolymerization of monomer **2** to **P2** is confirmed by the absence of aromatic signals ascribable to protons in α and α′-position of the thiophene ring (Fig. S4A). In particular, by the integral ratio of the aforementioned signals, centered at 2.81 ppm (HT dyads) and 2.57 ppm (HH and TT dyads), the regioregularity degree for **P1** can be then evaluated (70% of HT linkages). Similarly, the molar content of bromine (80%) and TPP (20%) can also be determined, since the resonances at 3.41 and 4.21 ppm can be exclusively ascribed to the protons of CH$_2$Br and CH$_2$O-TPP groups in the side chain, respectively. The success and rate of ionization with tributyl phosphine were then verified both by ^{1}H NMR and ^{31}P NMR spectroscopy. Firstly, the total absence of methylenic protons in α position to the bromine group as well as the presence of a broad signal at 2.21 and 2.27 ppm for **P1buP** (Fig. S3B) and **P2buP** (Fig. S4B), respectively, clearly shows the successful post-functionalization of both precursors. Those resonances can indeed be attributed to the eight methylenic protons near the cationic phosphine group. Besides, not only all the porphyrin content in **P1buP** is retained, but also both of the ^{31}P NMR spectra (Fig. S5-S6) confirm the complete absence of unreacted tributyl phosphine, as previously verified by ^{1}H NMR.

Finally, in the case of **P1buP-Zn** (Fig. S7), the disappearance of the signal at around 4.50 ppm, probably related to the resonance of the NH-pyrrolic subunits of the porphyrin moiety, confirms its successful and quantitative metalation with Zn^{2+}.

Table 2
Decomposition (T_d) and glass-transition (T_g) temperatures of ionic polymers.

	T_d (°C)[a]	T_g (°C)[b]
P1buP	237	76
P2buP	213	49

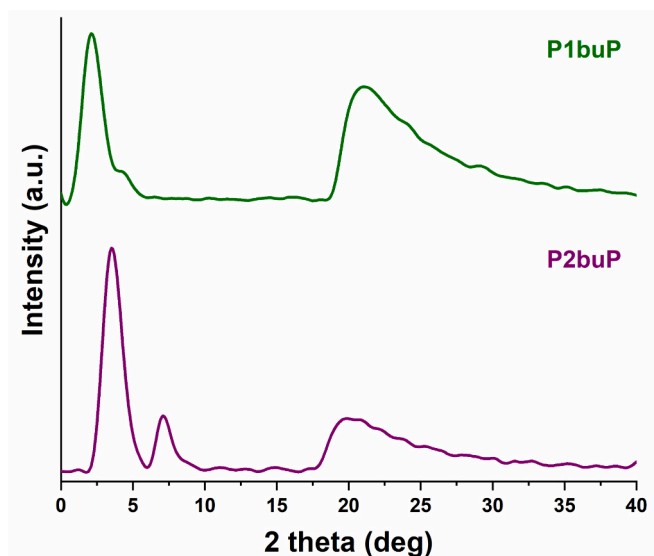[a] Determined by the onset point of the first inflection; [b] Evaluated by DSC analysis.

Fig. 2. X-ray diffractograms of **P1buP** and **P2buP**.

3.3. Thermal and XRD characterization

The thermal stability of the cationic polymers **P1buP** and **P2buP** was determined by TGA analyses, up to 600 °C and under an oxidizing atmosphere, while the thermal behavior was evaluated by DSC analyses, under a nitrogen atmosphere (Table 2, Fig. S8-S9).

When submitted to thermal treatment, both the ionic materials showed quite good resistance, displaying differences in the degradation pattern and several weight losses, at different temperature values (Fig. S8). The first weight loss can be both originated from the side chain degradation, involving a considerable weight decrease, with the highest percentage loss for **P2buP** (80%) in comparison to **P1buP** (40%). Indeed, despite the overall elimination of the phosphonium group for both materials, the ionic TPP-derivative clearly displays macromolecular stiffening and higher thermal stability in the solid state in

Table 3
Optical properties of the synthesized polymeric derivatives.

	Solvent	Solution λ_{max} (nm)[a]	Film λ_{max} (nm)[a]	E_g^{opt} (eV)[b]
P1	CHCl₃	420 *S-b*	431	
		449 *π-π**	482	2.12
		514, 552, 591, 646 *Q-b*	519, 554, 595, 651	
P2	CHCl₃	532	556, 601	1.92
P1buP	EtOH	420 *S-b*	427	
		451 *π-π**	481	2.23
		514, 551, 592, 649 *Q-b*	518, 553, 596, 652	
P1buP-Zn	EtOH	424 *S-b*	435 *S-b*	–
		558, 597 *Q-b*	565, 608 *Q-b*	
P2buP	EtOH	522	535	1.98

[a] Maximum absorption wavelength; [b] Optical energy band gap.

comparison with **P2buP**, probably due to the presence of strong dipolar interaction among the porphyrin-dye moiety. Finally, the weight losses up to 400–450 °C can be both ascribed to the starting decomposition of the macromolecular backbone. However, both **P1buP** and **P2buP** may be considered stable enough to be used as photoactive materials, since the degradation temperatures are higher than the exercise ones.

Concerning the thermal behavior (Fig. S9), both the examined samples show an endothermic flexure, ascribable to the glass transition temperature (T_g). The absence of melting and crystallization phenomena is therefore due to the substantially amorphous nature of the polymers. In fact, the steric hindrance of groups i.e., tributyl phosphonium and/or porphyrin moiety linked to the side chains presumably prevents the formation of crystallinity, as the conformational order of the polymeric chains decreases. Besides, the presence of a bulky and not flexible substituent such as porphyrin allows for significant increase in the T_g value, as reported in Table 2.

Fig. 2 shows XRD diffractograms of polymers in film at room temperature. The presence of two wide main peaks centered at 2θ = 2.15 and 3.49° and corresponding to the chain distance on the plain of 20.5 and 14.3 Å for **P1buP** and **P2buP**, respectively, suggests the existence of very small crystalline domains in their structure. The absence of any further evident peak in the wide-angle region of the diffractogram confirms the absence of any tridimensional array and then the predominantly amorphous nature of the films, as suggested by DSC analysis.

3.4. Optical properties

The optical properties of precursor and ionic polymers were evaluated by UV–Vis spectroscopy, in solid state (film on quartz) and in solution of CHCl₃ or different polar solvents (i.e., alcohols and water), respectively. The normalized absorption spectra are reported in Fig. 3,

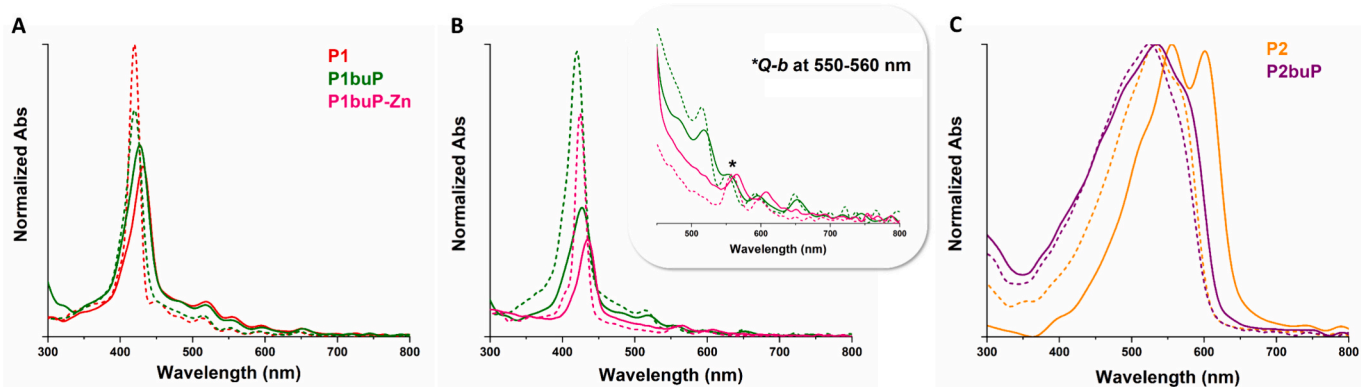

Fig. 3. Normalized UV–Vis spectra in solution (dashed line) and thin film (solid line) of precursor (in CHCl₃) and ionic polymers (in EtOH), normalized on the *π-π** maxima (A and C) or on the *Q-b* maxima at 550–560 nm (B).

Table 4
Electrochemical properties of ionic synthesized polymeric derivatives.

	E_{ox} (V)[b]	E_{red} (V)	HOMO (eV)[c]	LUMO (eV)[d]
P1buP	+0.84	–	−5.08	−2.85
P1buP-Zn	+0.82	–	−5.06	−2.83
P2buP	+0.53	–	−4.77	−2.79
C_{60}-Ser[a]	–	−0.37	–	−3.87

[a] As reported in ref. [42]; [b] Oxidation potential, determined in 0.1 mol L^{-1} $(C_4H_9)_4NClO_4$ in 25% CH_3CN, 75% toluene (C_7H_8), SCE absolute potential 4.24 eV; [c] HOMO $= -(E_{ox} + 4.24)$; [d] LUMO $= HOMO + E_g^{opt}$.

while their spectral data are reported in Table 3. Indeed, as ethanol (EtOH) proved to be the best compromise in terms of optical behavior and safety condition, only optical data in this solvent for **P1buP**, **P1buP-Zn** and **P2buP** are here reported. The behavior in all the other polar solvents can be additionally found in Fig. S10-S11 and Table S1-S2.

Except for **P2**, all materials show similar absorption profiles, both in solution and solid state. In the case of both the dye-sensitized thiophene-based copolymers (Fig. 3A), the typical absorptions of porphyrin electronic system are clearly shown, i.e. the intense Soret band (*S-b*) at about 420–430 nm, and the four weak Q-bands (*Q-b*) ranging from 510 to 650 nm [41]. Moreover, even though a partial overlapping with the porphyrin bands, the π-π* electronic transition of the conjugated polythiophene backbone is also visible, especially for **P1**, at around 450 nm (in solution) and 480 nm (in thin film). The poor dependence of the optical profiles from the kind of side chain, in addition to the modest shifts of λ_{max} passing from precursor (**P1**) to ionic material (**P1buP**), suggests that in this case the post-functionalization with more bulky groups, such as phosphonium salts, does not induce a substantial change in the optical behavior. Besides, despite the porphyrin moieties could probably affect the tendency of the polymeric backbone to assume more ordered and planar conformations, a clear band broadening in thin film is regardlessly displayed for both polymers. On the other hand, with the formation of the metal-porphyrin in **P1buP-Zn** (Fig. 3B), the *S-b* resulted to be substantially unchanged, but the four *Q-b* were collapsed in two bands, due to the increased symmetry of the system.

With regard to **P2**, in addition to being the most red-shifted, the thin-film absorption spectrum exhibits a quite evident vibronic structuration, probably due to strong inter- and intramolecular interactions (i.e., S—O non-covalent interaction), which provides a better planarity. Instead, by

post-functionalization, both the spectra of **P2buP** display a more featureless and slightly blue-shifted absorption. However, an enhanced band broadening and fine structuration are still obtained, especially in the solid state, thus assuming appreciable planarizing interactions (Fig. 3C).

The values of optical energy band gap (E_g^{opt}), which can be estimated by the onset absorption wavelength in thin film are also reported in Table 2. For a better comparison with **P2** and **P2buP**, the onset wavelength for **P1** and **P1buP** was also considered for the maximum absorption concerning the electronic transition of the conjugated polythiophene backbone. As expected, the results display a vivid bandgap decrease from ~2.10–2.20 eV to ~1.90–2.00 eV for the precursor/ionic dye-sensitized thiophene-based copolymer (**P1** and **P1buP**) and homo-poly(dialkoxythiophene) (**P2** and **P2buP**), respectively. Indeed, owing to the mesomeric effect, the stronger electron donor ability of double oxygen directly linked to the thiophene ring, as well as possible S—O non-covalent interaction, provide a remarkable bathochromic shift and thus reduce the energy band gap of the material.

By the obtained results, it can be noted that both couple of synthesized materials (**P1** with **P2** and **P1buP** with **P2buP**) clearly display complementary absorption profiles, thus suggesting the possibility of extending the light-harvesting capability when blended together. In particular, mixtures of **P1buP** and **P2buP**, in presence of a suitable EA material (i.e., an alcohol-soluble fullerene derivative), are therefore good candidates to be used as active layer in halogen-free ternary OSCs.

3.5. Electrochemical behavior

CV measurements were carried out on a thin film of all ionic materials prepared by drop-casting on Pt from ethanol solutions, in toluene/acetonitrile (75:25). The oxidation potentials as well as energy levels of polymers are reported in Table 4, while the related voltammograms in Fig. 4. In the case of **P1buP** and **P2buP** the fourth cycle was considered (Fig. 4A), while for **P1buP-Zn** only the second one was used (Fig. 4B), due to its overall enhanced solubility, as well as in the analysis mixture.

The oxidation potential was converted to the HOMO (highest occupied molecular orbital) energy, referring SCE to the ferrocene/ferrocenium internal reference. Since the evaluation of reduction potential – and therefore of the electrochemical band gap – was prevented by the absence of any evident peak in the negative bias range of CV curves, the LUMO (lowest unoccupied molecular orbital) energy was then indirectly calculated from the HOMO value and the optical band gap (E_g^{opt}, Table 3)
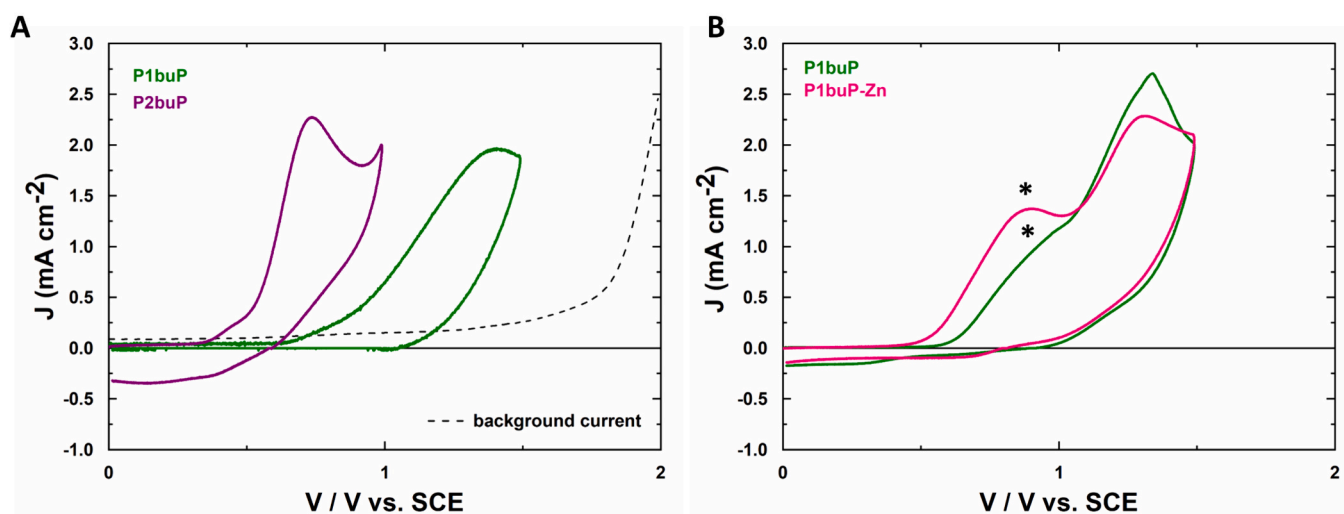
Fig. 4. (A) Fourth and (B) second cyclic voltammograms curves of ionic materials in thin film (* Oxidation process probably related to the bromine counterion).
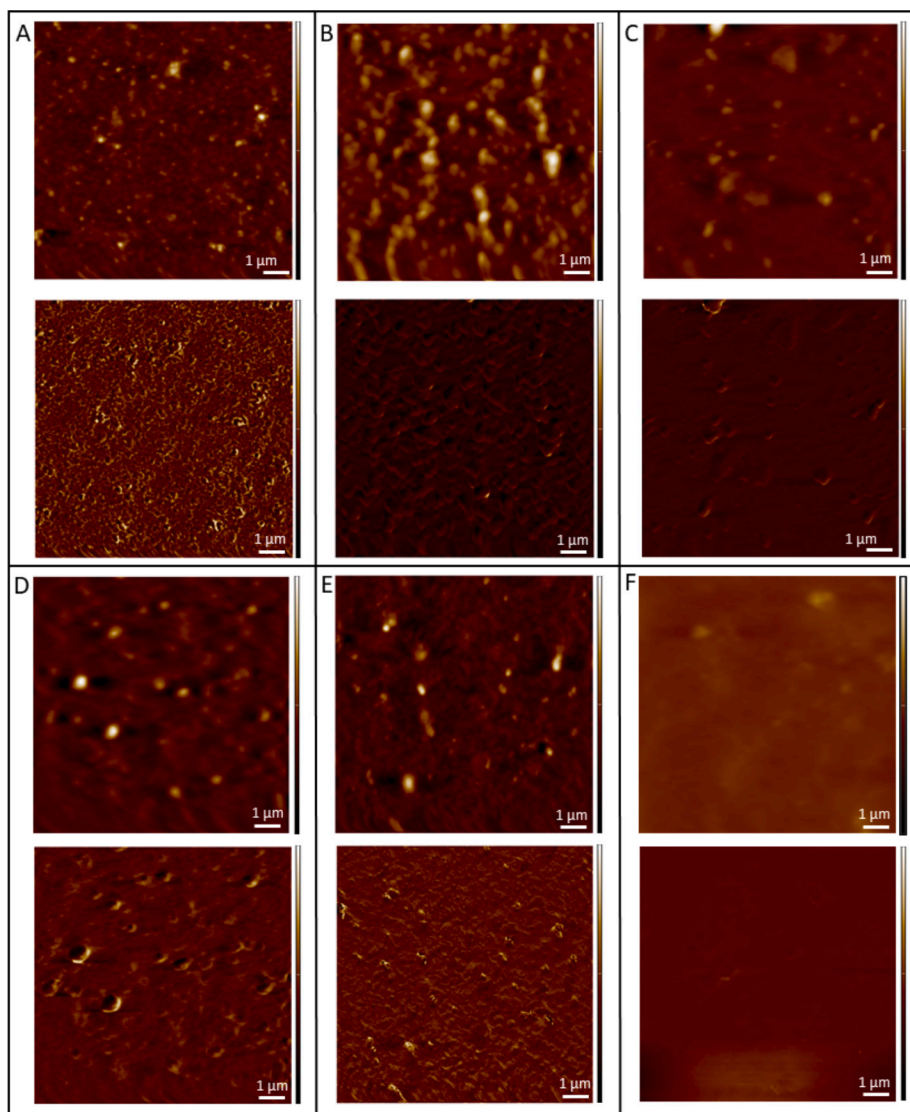
Fig. 5. Morphological structure of BHJ OSCs samples, showing their topology in the top row and phase images in the bottom row. A) $ED_1:ED_2:EA = 1:0:1$ sample, Z scale bars are 120 nm and 90°, respectively, and RMS 14.51 ± 3.4 nm; B) $ED_1:ED_2:EA = 0.67:0.33:1$ sample, Z scale bars are 250 nm and 25°, respectively, and RMS 30.17 ± 6.9 nm; C) $ED_1:ED_2:EA = 0.5:0.5:1$ sample, Z scale bars are 250 nm and 25°, respectively, and RMS 24.63 ± 5.1 nm; D) $ED_1:ED_2:EA = 0.33:0.67:1$ sample, Z scale bars are 100 nm and 10°, respectively, and RMS 11.26 ± 2.4 nm; E) $ED_1:ED_2:EA = 0:1:1$ samples, Z scale bars are 80 nm and 160°, respectively, and RMS 9.62 ± 1.9 nm; F) **P1buP** as cathode interlayer, Z scale bars are 150 nm and 100°, respectively, and RMS 10.31 ± 2.2 nm.

measured by the UV–Vis spectra in thin film.

It can be noted that the oxidation potential of **P2buP** is drastically reduced by the presence of oxygen conjugated in the side chain of thiophene rings, due to the ED effect of its *p*-orbital. On the other hand, the HOMO level energy of **P1buP** is very low if compared with **P2buP**, which is favorable for the obtainment of high open-circuit voltage (V_{oc}) in OSCs. As the E_g^{opt} of **P1buP-Zn** cannot be determined by the UV–Vis spectrum, despite the metalation process it can be reasonably assumed similar to the one of **P1buP**, since the TPP moiety is electronically insulated from the polyconjugated thiophene backbone. In fact, the oxidation potential resulted basically unchanged.

Therefore, this optimal cascade energy level alignment, in addition to having a reduced E_g^{opt} for **P2buP** and complementary abs profile, would suggest the use of these materials as suitable components in ternary OSCs. Moreover, due to their cationic nature and a fine matching with the energy levels of **P2buP:C$_{60}$-Ser** as binary host and the work functions of anode and cathode, the TPP derivatives might be also employed as cathode interlayers.

3.6. Morphology characterization

Therefore, to evaluate the interesting new concept of co-sensitization, different weight ratio blends of **P1buP** (ED_1) and **P2buP** (ED_2) with **C$_{60}$-Ser** (EA) were prepared and their morphological features in thin films investigated. AFM surface topography and phase images are provided in Fig. 5, from sample A to E, where the first row shows the images of sensitivity height, and the second one provides the phase images. Analogously, the topography of **P1buP** as cathode interlayer can be seen in Fig. 5F, combined with its phase image.

As it can be seen in Fig. 5A, the binary blend with TPP-copolymer and fullerene derivative ($ED_1:ED_2:EA = 1:0:1$) displays a relatively rough surface, where the irregularities can be seen all over the surface, with uniform height and size. Probably caused by a substantial aggregation of the two components, this can be further confirmed by the phase image, as the same pattern shows the changes in the phase of the surface. Fig. 5B, attributed to the $ED_1:ED_2:EA = 0.67:0.33:1$ blend, similarly shows another rough surface with bigger size roughnesses, as well as broader dispersion throughout the surface, maybe due to the

Table 5

Properties of BHJ OSCs prepared with alcohol-soluble materials **P1buP** (ED$_1$), **P2buP** (ED$_2$), and **C$_{60}$-Ser** (EA) (average values collected from 5 devices).

ED$_1$:ED$_2$: EA ratio	J_{sc} (mA•cm^{-2})[c]	J_{sc} (mA•cm^{-2})[d]	V_{oc} (V)[e]	FF[f]	PCE (%)[g]
1:0:1	4.5 ± 0.11	4.4 ± 0.18	0.59 ± 0.10	0.58 ± 0.02	1.53 ± 0.09
0.67:0.33:1	8.4 ± 0.13	8.3 ± 0.16	0.60 ± 0.11	0.58 ± 0.03	2.91 ± 0.12
0.5:0.5:1	12.1 ± 0.15	11.9 ± 0.19	0.61 ± 0.10	0.60 ± 0.03	4.45 ± 0.18
0.33:0.67:1	14.8 ± 0.17	14.7 ± 0.20	0.61 ± 0.12	0.58 ± 0.02	5.22 ± 0.19
0:1:1	11.1 ± 0.16	10.9 ± 0.15	0.55 ± 0.14	0.55 ± 0.02	3.37 ± 0.16
0:1:1[a]	12.3 ± 0.17	12.1 ± 0.15	0.65 ± 0.11	0.61 ± 0.05	4.88 ± 0.15
0:1:1[b]	14.2 ± 0.16	13.9 ± 0.21	0.58 ± 0.12	0.61 ± 0.04	5.03 ± 0.20

[a] With **PFN-Br** as commercial cathode interlayer; [b] With **P1buP** as cathode interlayer; [c] Short circuit current; [d] J_{sc} from EQE measurements; [e] Open circuit voltage; [f] Fill factor; [g] Photoconversion efficiency.

addition of the third component. Indeed, an overall similar trend is obtained with all ternary samples, but with fewer irregularities when the content of **P1buP** and **P2buP** decrease and increase, respectively. In particular, both Fig. 5C and D show fewer irregularities but bigger in size, as their scattered placements can be well seen in both phase images. On the other hand, the lowest Z scale bar for the sensitivity height was observed with the binary dialkoxy-fullerene blend (Fig. 5E), obtaining a smoother surface with less relative roughness compared to the other blends. In the end, when **P1buP** is used as cathode interlayer (Fig. 5F), the material shows relatively smooth surface, although the present irregularities have bigger sizes in contrast to their distance.

3.7. Photovoltaic properties

The possible role of **P1buP** as a third component was effectively investigated by the fabrication of halogen-free ternary BHJ organic solar cells, with an ITO/PEDOT:PSS/active layer/Al configuration. Similar to the morphology characterization, different weight ratio blends of **P1buP** (ED$_1$) and **P2buP** (ED$_2$) with **C$_{60}$-Ser** (EA) were thus employed as active layers. Besides, with the aim of investigating possible device engineering, **P1buP** was also tested as cathode interfacial materials in bicomponent BHJ devices, still made with the dialkoxy alcohol-soluble material as ED (ED$_2$:EA = 1:1 *w/w*). Ethanol is the solvent adopted to process all the materials. The photovoltaic performance parameters for all prepared devices are listed in Table 5, while the corresponding J–V features of the best-performing solar cells and external quantum

efficiency (EQE) curves are reported in Fig. 6.

3.7.1. Ternary OSCs vs interfacial engineering

According to the presented data, the two bicomponent BHJ OSCs devoid of any cathode interlayer provide quite different PCE values, with the dialkoxy alcohol-soluble material giving the best result when used as ED (Tables 5, 3.37%). Despite a slight reduction of the V_{oc} parameter, **P2buP** can provide a more extended coverage of the absorption spectrum (Fig. 6A), as well as a better LUMO level alignment with C$_{60}$-Ser as EA, probably ascribable to the presence of the two oxygroups, in addition to producing a smoother surface and less aggregates (Fig. 5E). Whereas the obtainment of high values of J_{sc} and thus PCE are prevented when **P1buP** is used as the only ED, likely due to the electronically insulated TPP moiety and its strong absorption but at lower wavelengths, not to mention its tendency to give aggregation with the EA counterpart (Fig. 5A). Particularly interesting are therefore the experimental findings obtained by the fabrication of the ternary OSCs. Not only do the three components maintain the alcohol soluble processability of the devices, but a substantial enhancement of the PCE value – ranging from ~4.5–5.2% – is guaranteed just with the ratio of 0.5:0.5:1 as ED$_1$:ED$_2$:EA. In particular, the best results were provided using the ratio of 0.33:0.67:1 with an improvement of PCE of 54% with respect to the best bicomponent device. Primarily originated by the high J_{sc} value and a good compromise of V_{oc} and FF parameters, this ratio clearly displays the best photoactive performance (Table 5 and Fig. 6B). Reasonably due to their complementary absorption profiles, an extended and well-structured light harvesting capability is produced (Fig. 6A), without compromising the film surface smoothing and homogeneity after blending (Fig. 5D).

It is also evident from Table 5 and Fig. 6, that **P1buP** is a valid and suitable candidate to be used as a cathode interlayer. With an improvement of PCE of 49% with respect to the reference device

Table 6

Comparison of photovoltaic performances of BHJ OSCs prepared with **P1buP** and **P1buP-Zn** (average values collected from 5 devices).

ED$_1$:ED$_2$:EA ratio	J_{sc} (mA•cm^{-2})[a]	J_{sc} (mA•cm^{-2})[b]	V_{oc} (V)[c]	FF[d]	PCE (%)[e]
1:0:1	4.5 ± 0.11	4.4 ± 0.18	0.59 ± 0.10	0.58 ± 0.02	1.53 ± 0.12
1*:0:1	4.9 ± 0.12	4.8 ± 0.16	0.59 ± 0.12	0.60 ± 0.01	1.72 ± 0.12
0.33:0.67:1	14.8 ± 0.18	14.7 ± 0.20	0.61 ± 0.11	0.58 ± 0.03	5.22 ± 0.21
0.33*:0.67:1	15.2 ± 0.16	14.9 ± 0.19	0.61 ± 0.10	0.65 ± 0.04	6.03 ± 0.19

*With **P1buP-Zn** as ED$_1$; [a] Short circuit current; [b] J_{sc} from EQE measurements; [c] Open circuit voltage; [d] Fill factor; [e] Photoconversion efficiency.
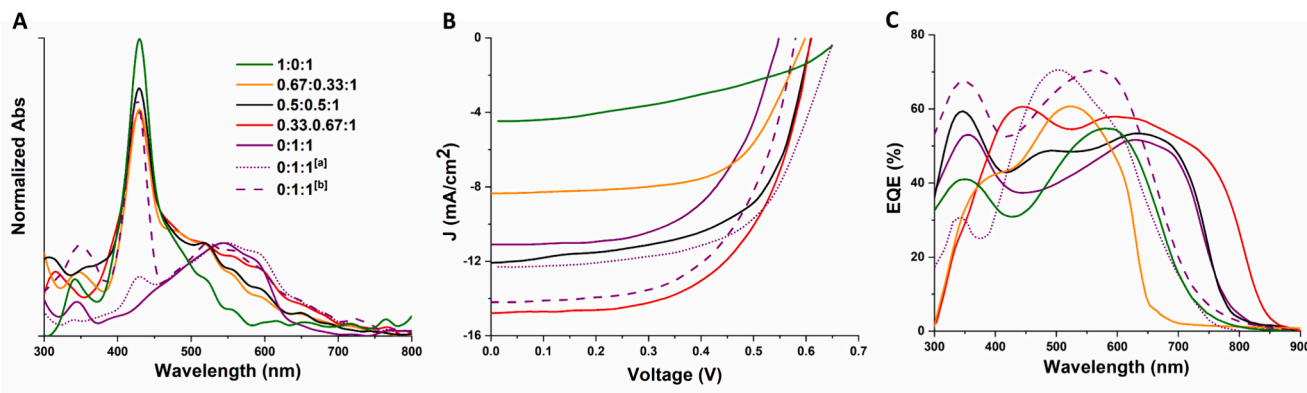
Fig. 6. A) Thin-film absorption spectra, B) J/V curves, and C) EQE curves of prepared BHJ OSCs.

(Table 5, 0:1:1 as ED$_1$:ED$_2$:EA), the obtained photovoltaic performances notably increase, resulting comparable and even better to device fabricated by using PFN-Br as a commercially available cathode interlayer. Indeed, the combination of porphyrin and ionic moieties seems to induce a reduction of the work function, with a slight enhancement of the V_{oc}, and a promotion of the electron injection to the Al cathode. The photo-current response curves (EQE curves, Fig. 6C) and related J_{sc} values (Table 5) of all investigated devices follow the values recorded, as well as the trend formerly observed in the absorption spectra, indicating that the whole absorption can effectively contribute to the photocurrent.

3.7.2. Optimization with Zn

Finally, to improve and optimize the best performing device, a portion of **P1buP** was successfully complexed with Zn^{2+} (**P1buP-Zn**, Scheme 1) and tested in ternary BHJ OSCs (Table 6, 0.33*:0.67:1 as ED$_1$: ED$_2$:EA). Indeed, due to the electronically-insulated nature of the TPP in P1buP-Zn, any substantial changes in the optical and electrochemical properties were prevented, but an overall improvement of its solubility in highly polar solvents was observed, thus suggesting a possible change in terms of thin film deposition/organization and therefore photo-activity. For a better understanding and study of the effect, the device with a bicomponent active layer with **P1buP-Zn** (Table 6, 1*:0:1) has also been fabricated. The morphological characterization by AFM technique of the obtained blends, as well as the J–V and external quantum efficiency (EQE) curves of the corresponding devices, are reported in Fig. S12 and S13, respectively.

Still maintaining an environmentally friendly approach, a rather clear improvement of ~15% of the performances was obtained. Indeed, mainly promoted by a further enhancement of the current density and fill factor, which is especially true for the ternary device, the best PCE value of 6% among all the experimental findings of this study was measured.

4. Conclusions

Efficient and completely halogen-free BHJ organic solar cells were fabricated using two polythiophenes functionalized with phosphonium salts at the end of their side chains, giving enhanced solubility in water-alcohol mixtures to the final materials. The first synthesized poly-thiophenic derivative (ED$_1$) was a copolymer composed of ionic and tetraphenylporphyrin-dye functionalized units, while the second one (ED$_2$) was a disubstituted homopolymer bearing the ionic group at the end of hexamethylenic side chains linked to the main polythiophenic chain through oxygen atoms. The two polymers were fully characterized and tested as photoactive donor materials in combination with an alcohol-soluble fullerene derivative (EA) to prepare ternary solar cells. Results indicate that the ternary cells are effective in complementing absorption spectra, optimizing the electronic energy level gradient, and homogenizing the external surface of the device. As a result, the OSC with a ED$_1$:ED$_2$:EA weight ratio of 0.33:0.67:1 exhibits a PCE of 5.22%, a value that further increases (6.03%) when porphyrin is complexed with Zn without affecting the solubility and film ability of the active blend. Moreover, to investigate a possible device engineering process, the ionic TPP material was also investigated and tested as an alcohol-soluble cathode interlayer.

CRediT authorship contribution statement

Martina Marinelli: Writing – review & editing, Writing – original draft, Validation, Methodology, Investigation, Data curation, Conceptualization. **Massimiliano Lanzi:** Writing – review & editing, Supervision, Resources, Methodology, Investigation, Funding acquisition. **Debora Quadretti:** Validation, Methodology, Investigation. **Yasamin Ziai:** Writing – review & editing, Investigation, Data curation. **Filippo Pierini:** Writing – review & editing, Investigation, Data curation. **Alberto Zanelli:** Writing – review & editing, Investigation, Data curation. **Riccardo Medri:** Investigation, Data curation. **Elisabetta Salatelli:** Writing – review & editing, Supervision, Investigation, Funding acquisition.

Declaration of competing interest

The authors declare that they have no known competing financial interests or personal relationships that could have appeared to influence the work reported in this paper.

Data availability

Data will be made available on request.

Appendix A. Supplementary data

Additional supporting information (synthesis of 6-bromo-1-hexanol (**B6OH**), 3,4-(6,6′-bromohexyloxy)thiophene (**2**), poly{3-(6-bromo-hexyl)thiophene-co-3-[5-(4-phenoxy)-10,15,20-triphenylporphyrinyl] hexylthiophene} (**P1**), poly[3,4-(6,6′-bromohexyloxy)thiophene] (**P2**), poly{3-(6-tributylphosphoniumhexyl)thiophene-co-3-[5-(4-phenoxy)-10,15,20-triphenylporphyrinyl]hexylthiophene bromide} (**P1buP**), and poly[3,4-(6,6′-tributylphosphoniumhexyloxy)thiophene] bromide] (**P2buP**); metalation procedure; NMR spectra of intermediates, monomers and polymers; TGA and DSC thermograms of ionic polymers; UV–Vis and PL data/spectra of ionic polymers; morphology and photoactive characterization of **P1buP-Zn**) can be found in the online version of this article at the publisher's website.

References

[1] S. Gressler, F. Part, S. Scherhaufer, G. Obersteiner, M. Huber-Humer, Sist. Mater-Tecj. 34 (2022) e00501.
[2] Y. Lu, G. Xu, C. Cui, Y. Li, Flexible and semitransparent organic solar cells, Adv. Energy Mater. 8 (7) (2018) 1701791.
[3] S.Y. Chang, P. Cheng, G. Li, Y. Yang, Transparent polymer photovoltaics for solar energy harvesting and beyond, Joule 2 (6) (2018) 1039–1054.
[4] S. Li, C.Z. Li, M. Shi, H. Chen, New phase for organic solar cell research: emergence of Y-series electron acceptors and their perspectives, ACS Energy Lett. 5 (5) (2020) 1554–1567.
[5] A. Wadsworth, Z. Hamid, J. Kosco, N. Gasparini, I. McCulloch, The bulk heterojunction in organic photovoltaic, photodetector, and photocatalytic applications, Adv. Mater. 32 (38) (2020) 2001763.
[6] Y. Cui, H.F. Yao, J.Q. Zhang, K.H. Xian, T. Zhang, L. Hong, Y.M. Wang, Y. Xu, K. Q. Ma, Single-junction organic photovoltaic cells with approaching 18% efficiency, Adv. Mater. 32 (19) (2020) 1908205.
[7] L. Zhan, S. Li, X. Xia, Y. Li, X. Lu, L. Zuo, M. Shi, H. Chen, Layer-by-layer processed ternary organic photovoltaics with efficiency over 18%, Adv. Mater. 33 (12) (2021) 2007231.
[8] N.Y. Doumon, L. Yang, F. Rosei, Ternary organic solar cells: a review of the role of the third element, Nano Energy 94 (2022) 106915.

[9] C. Lee, S. Lee, G.U. Kim, W. Lee, B.J. Kim, Recent advances, design guidelines, and prospects of all-polymer solar cells, Chem. Rev. 119 (13) (2019) 8028–8086.

[10] A. Karki, A.J. Gillett, R.H. Friend, T.Q. Nguyen, The path to 20% power conversion efficiencies in nonfullerene acceptor organic solar cells, Adv. Energy Mater. 11 (15) (2021) 2003441.

[11] Y. Sun, T. Liu, Y. Kan, K. Gao, B. Tang, Y. Li, Flexible organic solar cells: progress and challenges, Small Sci. 1 (15) (2021) 2100001.

[12] S. Rasool, J. Yeop, H.W. Cho, W. Lee, J.W. Kim, D. Yuk, J.Y. Kim, Path to the fabrication of efficient, stable and commercially viable large-area organic solar cells, Mater. Fut. 2 (2023) 032102.

[13] V. Piradi, F. Yan, X. Zhu, W.Y. Wong, A recent overview of porphyrin-based π-extended small molecules as donors and acceptors for high-performance organic solar cells, Mater. Chem. Front. 5 (19) (2021) 7119–7133.

[14] K. Gao, Y. Kan, X. Chen, F. Liu, B. Kan, L. Nian, X. Wan, Y. Chen, X. Peng, T. P. Russell, Y. Cao, A.K.-Y. Jen, Low-bandgap porphyrins for highly efficient organic solar cells: materials, morphology, and applications, Adv. Mater. 32 (32) (2020) 1906129.

[15] A. Soultati, M. Verouti, E. Polydorou, K.-K. Armadorou, Z. Georgiopoulou, L. C. Palilis, I. Karatasios, V. Kilikoglou, A. Chroneos, A.G. Coutsolelos, P. Argitis, M. Vasilopoulou, Efficient and stable air-processed ternary organic solar cells incorporating gallium-porphyrin as an electron cascade material, Nanomaterials 13 (2023) 2800.

[16] M.A. Ochieng, J.F. Ponder, J.R. Reynolds, Effects of linear and branched side chains on the redox and optoelectronic properties of 3, 4-dialkoxythiophene polymers, Polym. Chem. 11 (12) (2020) 2173–2181.

[17] S. Ming, Z. Li, S. Zhen, P. Liu, F. Jiang, G. Nie, J. Xu, High-performance DAD type electrochromic polymer with π spacer applied in supercapacitor, J. Chem. Eng. 390 (2020) 124572.

[18] L. Chang, M. Sheng, L. Duan, A. Uddin, Ternary organic solar cells based on non-fullerene acceptors: a review, Org. Electron. 90 (2021) 106063.

[19] C. Zhao, J. Wang, X. Zhao, Z. Du, R. Yang, J. Tang, Recent advances, challenges and prospects in ternary organic solar cells, Nanoscale 13 (4) (2021) 2181–2208.

[20] M. Vartanian, P. De La Cruz, S. Biswas, G.D. Sharma, F. Langa, Panchromatic ternary organic solar cells with 9.44% efficiency incorporating porphyrin-based donors, Nanoscale 10 (15) (2018) 12100–12108.

[21] V. Piradi, X. Xu, Z. Wang, J. Ali, Q. Peng, F. Liu, X. Zhu, Panchromatic ternary organic solar cells with porphyrin dimers and absorption-complementary benzodithiophene-based small molecules, ACS Appl. Mater. Interfaces 11 (6) (2019) 6283–6291.

[22] R. Sorrentino, E. Kozma, S. Luzzati, R. Po, Interlayers for non-fullerene based polymer solar cells: distinctive features and challenges, Energy Environ. Sci. 14 (1) (2021) 180–223.

[23] J. Hong, D. Zhang, H. Kwon, C.E. Park, S.K. Kwon, Y.H. Kim, A solution-processed cathode interfacial layer facilitates efficient energy level alignment in organic photovoltaics, J. Phys. Chem. C 125 (36) (2021) 20067–20075.

[24] M. Tountas, A. Verykios, E. Polydorou, A. Kaltzoglou, A. Soultati, N. Balis, P. A. Angaridis, M. Papadakis, V. Nikolaou, F. Auras, L.C. Palilis, D. Tsikritzis, E. K. Evangelou, S. Gardelis, M. Koutsoureli, G. Papaioannou, I.D. Petsalakis, S. Kennou, D. Davazoglou, P. Argitis, P. Falaras, A.G. Coutsolelos, M. Vasilopoulou, Engineering of porphyrin molecules for use as effective cathode interfacial modifiers in organic solar cells of enhanced efficiency and stability, ACS Appl. Mater. Interfaces 10 (2018) 20728–20739.

[25] K. Bini, X. Xu, M.R. Andersson, E. Wang, Alcohol-soluble conjugated polymers as cathode interlayers for all-polymer solar cells, ACS Appl. Energy Mater. 1 (5) (2018) 2176–2182.

[26] Y. Shi, X. Lu, Y. Zhang, J. Xi, Efficient polymer solar cells that use conjugated polyelectrolyte with a tetravalent amine-end side chain, Org. Electron. 77 (2020) 105542.

[27] C. Feng, X. Wang, G. Chen, B. Zhang, Z. He, Y. Cao, Mechanism of the alcohol-soluble ionic organic interlayer in organic solar cells, Langmuir 37 (14) (2021) 4347–4354.

[28] M. Marinelli, M. Lanzi, A. Liscio, A. Zanelli, M. Zangoli, F. Di Maria, E. Salatelli, Single-material organic solar cells with fully conjugated electron-donor alkoxy-substituted bithiophene units and electron-acceptor benzothiadiazole moieties alternating in the main chain, J. Mater. Chem. C 8 (2020) 4124–4132.

[29] L. Angiolini, T. Benelli, V. Cocchi, M. Lanzi, E. Salatelli, Side chain porphyrin moiety linked to polymer-fullerene composite solar cell, React. Funct. Polym. 73 (2013) 1198–1206.

[30] M. Lanzi, D. Quadretti, M. Marinelli, Y. Ziai, E. Salatelli, F. Pierini, Influence of the active layer structure on the photovoltaic performance of water-soluble polythiophene-based solar cells, Polymers 13 (2021) 1640.

[31] X. Chen, Q. Qu, Synthesis and optoelectrochemical properties of a magenta-to-transmissive electrochromic polymer based on 3, 4-dioxythiophene, Sol. Energy Mater. Sol. Cells 179 (2018) 270–275.

[32] J. Chang, S.-J. Zhang, Y.-W. Jiang, L. Xu, J.-M. Yu, W.-J. Zhou, X. Sun, Design, synthesis, and antibacterial activity of demethylvancomycin analogues against drug-resistant Bacteria, ChemMedChem 8 (6) (2013) 976–984.

[33] M. Lanzi, E. Salatelli, M. Marinelli, F. Pierini, Effect of photocrosslinking of D-A thiophene copolymers on the performance of single-material solar cells, Macromol. Chem. Phys. 221 (2020) 1900433.

[34] S. Hladysha, A. Murmiliuka, J. Vohlídala, D. Havlíčekb, V. Sedlaříkc, M. Štěpáneka, J. Zedníka, Combination of phosphonium and ammonium pendant groups in cationic conjugated polyelectrolytes based on regioregular poly(3-hexylthiophene) polymer chains, Eur. Polym. J. 100 (2018) 200–208.

[35] C. He, Q. He, C. Deng, L. Shi, D. Zhu, Y. Fu, H. Cao, J. Cheng, Turn on fluorescence sensing of vapor phase electron donating amines via tetraphenylporphyrin or metallophenylporphyrin doped polyfluorenew, Chem. Commun. 46 (2010) 7536–7538.

[36] D.R. Martir, D. Averardi, D. Escudero, D. Jacqueminb, E. Zysman-Colman, Photoinduced electron transfer in supramolecular ruthenium–porphyrin assemblies, Dalton Trans. 46 (2017) 2255–2262.

[37] M. Kumada, K. Tamao, Aliphatic organopolysilanes, Adv. Organomet. Chem. 6 (1968) 19–117.

[38] J. Pommerehne, H. Vestweber, W. Guss, R.F. Mahrt, H. Bassler, M. Porsch, J. Daub, Adv. Mater. 7 (6) (1995) 551–554.

[39] B.W.D. Andrade, S. Datta, S.R. Forrest, P. Djurovich, E. Polikarpov, M. E. Thompson, Relationship between the ionization and oxidation potentials of molecular organic semiconductors, Org. Electron. 6 (2005) 11–20.

[40] S. Hladysha, A. Murmiliuka, J. Vohlídala, D. Havlíčekb, V. Sedlaříkc, M. Štěpáneka, J. Zedníka, Combination of phosphonium and ammonium pendant groups in cationic conjugated polyelectrolytes based on regioregular poly(3-hexylthiophene) polymer chains, Eur. Polym. J. 100 (2018) 200–208.

[41] V. Piradi, F. Yan, X. Zhu, W.-Y. Wong, A recent overview of porphyrin-based p-extended small molecules as donors and acceptors for high-performance organic solar cells, Mater. Chem. Front. 5 (2021) 7119.

[42] M. Marinelli, M. Lanzi, F. Pierini, Y. Ziai, A. Zanelli, D. Quadretti, F. Di Maria, E. Salatelli, Ionic push–pull polythiophenes: a further step towards eco-friendly BHJ organic solar cells, Polymers 14 (2022) 3965.